Journal of
Composites Science

MDPI

Article

In Situ Synthesis, Characterization and Photocatalytic Efficacy of Silver-Enhanced MXene and Graphene Nanocomposites

Kishore Chand [1,*], M. Mustafa Azeem [2], Muhammad Nazim Lakhan [3], Mukhtiar Ahmed [4], Muhammad Jehanzaib Aslam [5] and Ahmer Hussain Shah [6]

[1] Key Laboratory of In-Fiber Integrated Optics, College of Physics and Optoelectronic Engineering, Harbin Engineering University, Harbin 150001, China
[2] Department of Nuclear Engineering & Radiation Science, Missouri University of Science and Technology, Rolla, MO 65409, USA; mustafa@mst.edu
[3] Applied Chemistry and Environmental Science, School of Science, STEM College, RMIT University, Melbourne, VIC 3000, Australia; s3954608@student.rmit.edu.aurmit
[4] State Key Laboratory of Multiphase Complex Systems, Institute of Process Engineering, Chinese Academy of Sciences, University of Chinese Academy of Sciences, Beijing 100190, China; ahmedmukhtiar461@mails.ucas.ac.cn
[5] Department of Physics, Florida Agriculture and Mechanical University, Tallahassee, FL 32309, USA; muhammad1.aslam@famu.edu
[6] Department of Textile Engineering & Design, Balochistan University of Information Technology, Engineering and Management Sciences, Quetta 87300, Pakistan; ahmer.shah@buitms.edu.pk
* Correspondence: kishor.vallasai@hrbeu.edu.cn or kishor.vallasai@gmail.com

Abstract: The emergence of 2D materials has significantly expanded the wide range of nanomaterials with diverse applications. Notably, their high conductivity, catalytic efficiency, and hydrophobicity have fueled heightened research interests for water treatment applications. This research aimed to investigate the synthesis and characterization of MXene and reduced graphene oxide (rGO) nanocomposites with silver nanoparticles (Ag) for enhanced catalytic activity in the decomposition of Direct Blue-24 dye. In this study, we employed well-established methods, previously documented in the literature, to prepare two distinct nanocomposites. Novel nanocomposites, namely reduced graphene oxide–silver nanoparticles (rGO–Ag) and MXene–silver nanoparticles (MXene–Ag), were synthesized using the hydrothermal and direct reduction method with an ammoniacal solution (aqueous solution). Comprehensive characterization using advanced tools revealed that the introduced Ag particles integrated seamlessly onto the parent nanofilms of the Carbon derivatives, forming a secondary phase with enhanced catalytic functionality. These nanocomposites demonstrated significant improvements in the catalytic decomposition reactions in simulated wastewater. Verification involved the reduction reaction of Direct Blue-24 dye at known nanocomposite concentrations. The results indicated that MXene–Ag exhibited a superior catalytic activity of 98% in 10 min compared to the rGO–Ag nanocomposite films, which achieved 96% in 35 min. The results indicated that MXene–Ag nanocomposites exhibited a 20–25% increase in catalytic efficiency compared to the rGO–Ag nanocomposites. The outcomes of this research hold promise for practical applications in textile wastewater management and various industrial sectors dealing with mutagenic and carcinogenic chemicals containing azo and/or phthalocyanine products.

Keywords: MXene; MXene–silver nanocomposite; reduced Graphene oxide–silver nanocomposite; photocatalytic decomposition; Direct Blue-24 dye

Citation: Chand, K.; Azeem, M.M.; Lakhan, M.N.; Ahmed, M.; Aslam, M.J.; Shah, A.H. In Situ Synthesis, Characterization and Photocatalytic Efficacy of Silver-Enhanced MXene and Graphene Nanocomposites. *J. Compos. Sci.* **2024**, *8*, 243. https://doi.org/10.3390/jcs8070243

Academic Editor: Sambandam Anandan

Received: 10 May 2024
Revised: 17 June 2024
Accepted: 19 June 2024
Published: 26 June 2024

1. Introduction

In this modern era, researchers are focusing on the discovery of advanced materials like Graphene, Graphene oxide, MXene, metal nanoparticles (NPs) and their composites, which have unique properties and advanced applications including electrical, catalytic, optical and antibacterial, etc. [1–4]. Many researchers are focusing on metal NPs worldwide

in different fields of material science, chemistry, physics, and nanotechnology as well as in biological sciences [5,6]. Metal NPs are widely used in a variety of applications; among all the metals, silver nanoparticles (AgNPs) show superior catalytic and antibacterial properties [5,7]. AgNPs exhibit the advantages of good heat resistance, sterilization durability, and broad-spectrum antimicrobial resistance as sterilizing reagents [8]. Metal NPs can be prepared using various methods like biological, physical, and chemical methods. The functionalization of NPs is more important. Functionalizing NPs with suitable materials can improve the catalytic and biocompatibility properties of NPs, among these, in situ is a chemical method of the preparation of composite materials such as AgNPs with Graphene and MXene, which is widely used as well as being a low-cost method [9,10].

Graphene is a most promising nanomaterial since its discovery in 2004 [11], due to its unique catalytic, electrical and optical performance properties along with its physical properties including mechanical strength and large specific surface area [12]. It is a cheap, renewable and easily obtained nanomaterial when compared to other materials [13]. Graphene is a 2D honeycomb structure material with an Sp^2-bonded single layer of carbon atoms arranged in a hexagonal pattern [14], also known as the mother of all graphitic carbon materials due to its building block. Graphene is a carbon material that has a different dimension like 0D, 1D, and 3D fullerenes, carbon nanotubes and graphite, respectively. While Graphene normally refers to the single layer of Sp^2-bonded carbon atoms, there are bi and few-layered Graphene as well [15]. Graphene shows outstanding properties such as electrical, thermal, and optical conductivity, high specific surface area, excellent mechanical properties, excellent charge transport mobility, high density, high electrocatalytic activity, desirable biocompatibility and low cost, etc. [15–19].

A Graphene oxide (GO) material can be synthesized using various techniques like mechanical exfoliation, chemical vapor deposition, electrical arc discharge techniques and epitaxial growth, and chemical vapor deposition (CVD) [20–22]. Among all these techniques, the hydrothermal process is highly efficient because of its ease [23–25]. GO as a single-layered insulating material can exhibit more properties by reducing it to rGO using different methods. Different chemicals like hydroquinone [26], hydrazine derivative [27], sodium borohydride [28], and hydrogen iodide [29,30] were widely used for the reduction of GO but sodium bisulfate along with silver nitrate solution is an efficient method for composite material manufacturing [31–33].

Another 2D material, MXene, was discovered in 2011. MXene can be synthesized simply by etching MXene into the hydrogen fluoride solution. It contains a large number of active groups like a fluorine ion, an oxygen group and a hydroxyl group on the surface with electronic force [34–36]. MXene is also very popular because of its unique mechanical, electrical, and optical properties. It is an advanced material with the same structure of Graphene and has a wide range of applications in the field of catalysts, energy storage, sensors, adsorption, hydrogen storage, and biological applications, etc. [37,38]. It has also been one of the most popular materials in the field of functional materials in recent years. MXene, is basically a MAX phase etching material, and has ternary-layered nitride or carbide materials with properties of both ceramics and metals [39,40]. It has a formula of $M_{(n+1)}AX_{n,}$, where M, A, and X represent the transition metal element, group IIIA or IVA elements, nitrogen and carbon elements, respectively, and n can be one, two or three. A hexagonal crystal structure, MAX has M, a packed layer, X atoms are filled in the M and the M layer is dispersed into the A layer between them, i.e., M-A and M-X are the covalent/metal/ion bond and the covalent bond, respectively. As a layered material, MXene can be achieved by simply etching away the Al layer using MAX [39,41–45].

Silver nanoparticles (AgNPs) properties depend on the stability of the NPs and also on their shape and size. However, unfunctionalized AgNPs can easily be agglomerated and are not stable. Functionalizing AgNPs with suitable materials can improve the catalytic and biocompatibility properties of AgNPs [46,47]. In recent years, special attention has been paid to AgNPs, rGO and MXene through different kinds of synthesis methods to produce various types of rGO–Ag and MXene–Ag composites for a wide range of applications in the

fields of catalytic, biomedical and energy sectors [39,48,49]. However, various MX–Ag and rGO–Ag nano composites effectively prevented aggregation and maintained the stability of NPs in water. Additionally previous synthesis methods for MXene–Ag and rGO–Ag nano composites were time-consuming, complex, or involved toxic chemicals or surfactants.

According to the previous literature, GO/rGO and MXene with different metal nanocomposites already presented excellent properties. Stability and hydrophilic properties can be achieved using different composite materials and catalytic efficiency can be increased. In nanocatalyst studies, stability is the major issue that can be prevented by fictionalizations of NPs [50]. Alternatively, Ag–rGO, MXene–Ag, and MXene–Fe_2O_3 synthesized using different methods showed excellent properties as a nanocatalyst, and for energy storage, antibacterial and other applications. It is also possible that the properties of rGO and MXene can be enhanced by the combination of different materials [51]. The dying industries use dyes that need sufficient treatment of water after their use; for that, it is also very important to purify wastewater with a suitable treatment [52]. Most of the dyes are mutagenic, carcinogenic as well as very harmful to living organisms such as animals and plants, etc. Direct Blue (DB)-24 is of a common class that is widely used in the dyeing industry.

This study presents the synthesis of reduced Graphene oxide–silver nanoparticles (rGO–Ag) and modified MXene–silver nanoparticle (MXene–Ag) nanocomposites uniformly anchored on the surface of MXene and rGO substrates to promote the improvement of catalytic activity. The synthesized products were characterized using advanced techniques like XRD, TEM, AFM, and XPS. All the results showed that the approach was suitable for preparing rGO, MXene, rGO–AgNPs, and MXene–AgNPs-based nanocomposites. Furthermore, rGO, MXene, rGO–AgNPs, and MXene-AgNPs were used for catalytic application for DB-24 dye. These well-prepared composites showed excellent performance for the dye decomposition of DB-24 as a model dye. This work on composites of rGO–Ag and MXene–Ag demonstrated a new direction for the research of MXene and rGO and nanocomposite catalysts for DB-24 dye. To the best of our knowledge, there are few reports on the use of rGO, MXene, rGO–AgNPs, and MXene–AgNPs nanocomposites for the decomposition of DB-24. Additionally, we presented a comparative study between rGO–AgNPs and MXene–AgNPs for catalytic activity against the decomposition of DB-24 dye. The selection of MXene and graphene-based nanocomposites with silver nanoparticles for catalytic applications is motivated by their exceptional properties such as high conductivity, catalytic efficiency, and hydrophobicity, making them promising candidates for water treatment applications. The novelty of this study lies in the synthesis and characterization of MXene–Ag and rGO–Ag nanocomposites, demonstrating their superior catalytic activity in degrading Direct Blue-24 dye under solar light irradiation, with MXene–Ag showing a 25% increase in catalytic efficiency compared to rGO–Ag.

2. Materials and Methods

2.1. Materials Selection

All chemicals, as mentioned in Table 1, were obtained from the most reputable company in China (Aladdin reagent Co., Ltd, Shanghai, China) and were used as received.

2.2. Preparation of Ammoniacal Solutions

Ammoniacal solution was prepared according to the literature [9]. In detail, 1.5 mL silver nitrate solutions were taken into the beaker, then after 2–3 drops of ammonia were added to this a black precipitation was formed and disappeared by addition of more ammonium hydroxide. After that, 5 mL of 3%-NaOH was added, again the same precipitation was formed, and disappeared by adding ammonia dropwise until the color of solution became opalescent, and some amount of distilled water was added to make it up to 50 mL volume. The solution was filtered and kept for further use.

Table 1. Materials used in the experimental procedure.

S.No	Materials	Purity (%)
1.	Graphite powder	99.95% and 4000 mesh size
2.	Silver nitrate ($AgNO_3$)	99.9%
3.	Titanium	98%
4.	Carbon	99%
5.	Aluminum	98%
6.	Sulfuric acid (H_2SO_4)	Concentrated
7.	Sodium boro hydride ($NaBH_4$)	97%
8.	Hydrochloric acid (HCl)	Concentrated
9.	Sodium hydroxide (NaOH)	99%
10.	Potassium permanganate ($KMnO_4$)	97%
11.	Ammonium hydroxide-28% (NH_4OH)	25–28%
12.	Sodium nitrate ($NaNO_3$)	99.8%
13.	Sodium bisulfate ($NaHSO_4$)	98.5–100%
14.	Hydrogen peroxide (H_2O_2)	30%
15.	Direct Blue dye ($C_{34}H_{22}N_6Na_4O_{16}S_4$)	≥98%

2.3. Synthesis of GO

GO was prepared using modified Hummers method from pure graphite powder [31]. In general, 70 mL sulfuric acid (H_2SO_4-concentrated 0.995 to 1.005 N) and 0.5 g of $NaNO_3$ were mixed and stirred for several mins; after that, 1 g graphite powder was added slowly and gradually for 1 h and kept stirring till that total graphite powder is mixed with solution. Potassium permanganate ($KMnO_4$) was then added dropwise with continuous stirring till the solution turned completely green. After that, the solution was transferred to water bath at 35 °C and left for stirring for 2 h and again beaker was transferred to ice bath and 100 mL water was poured into the solution dropwise. After this stage, the solution was transferred to water bath at 85 °C for stirring for 30 min. Finally, 17 mL of H_2O_2 and 83 mL of distilled water were poured into the solution and left stirring for 20 min. The color of the solution changed from dark green to yellow and 27 mL of HCl and 73 mL of distilled water were mixed into this solution for washing the residual. Then, the supernatant was decanted away, and the washed GO was dried into the ice bath and dried GO sheets were collected after 3 days.

2.4. Synthesis of rGO–Ag Nanocomposite

Reduced graphene oxide and silver nano composite were prepared using hydrothermal method [9]. Firstly, the solution of 40 mM [Ag $(NH_3)_2$]OH (silver ammonia) was prepared by titration of $AgNO_3$ solution with 1 wt.% NH_4OH solution in the dark. GO dispersion (3 mg/mL, 80 mL) was stirred for 5 h and then mixed with $NaHSO_3$ solution (0.41 mmol L^{-1}, 10 mL) using sonication for 5 min. Thereafter, 1 mL of [Ag $(NH_3)_2$] OH) solution was added into the GO suspension dropwise under sonication for 15 min. The resulting suspension was transferred into 100 mL Teflon-lined autoclave and the mixture was heated for 8 h at 180 °C for the synthesis of rGO–Ag. After that, obtained rGO–Ag was washed and dried in ice bath and used for further characterization and catalytic application.

2.5. MAX (Ti_3AlC_2) and MXene Preparation

MXene (Ti_3AlC_2) was prepared according to the literature [39]. The obtained MAX phase was applied for the MXene preparation using selective etching of group A from the phase of MAX into the hydrogen fluoride (HF-40%) followed in the literature [41] at room temperature for 10 h. After this treatment, the solution was centrifuged and obtained solution was washed with distilled water till the pH level of solution reached 6 as the MXene sediments should be washed otherwise impurities or residual MXene will affect the properties of MXene. The as-obtained material was dried and used for further processing.

2.6. MXene–Ag Nanocomposite Preparation

MX–Ag nanocomposites were prepared according to the literature [39,48,49]. In detail, 100 mg MXene powder was dispersed into 80 mL of distilled water and left for ultra-sonication for 5 h to obtain uniform suspension. Thereafter, the solution of 15 mL ammoniacal solution[$Ag(NH_3)_2$]OH was injected dropwise into the MXene suspension with continuous stirring. After that, obtained solution of MXene–Ag was centrifuged and washed with ethyl alcohol and dried in ice bath and used for further characterization and for catalytic application.

2.7. Characterization

The crystalline nature of nanoparticles was determined using XRD Rigaku TTR at 40 KV and 150 mA in range 2θ area between 20 and 800° with intensity of Cu-Ka (λ) radiation around 0.15406 nm. Particle size was determined using Scherrer Equation (1).

$$\tau = \frac{k\,\lambda}{\beta\,cos\theta} \quad (1)$$

where k indicates shape factor with a constant value of 0.9, λ is the wavelength (radian), β is the FWHM (radian), θ is diffraction angle and τ is average NPs.

High-resolution TEM (HRTEM), Transmission electron microscopy (TEM), and Eds mapping were used to quantify morphology and size of particles. TEM; FEI Technai G2 instrument (FEI, Hillsboro, OR, USA) was used to find out the elemental composition of AgNPs. Software Nano Measure (version 1.2) was used for obtaining the particle size distribution histogram. UV-Vis (Model: Perkin Elmer Lamda 35, Hamburg, Germany) was used to study catalytic decomposition process and determine the optical absorption of dye solutions using nanocatalyst keeping range of 200–800 nm. Furthermore, the surface morphology of the green synthesized AgNPs was recorded using AFM a Keysight equipment Model 5500 (Keysight Technologies, Chandler, AZ, USA). XPS (VG Scientific Co. Ltd, London, UK, ESCALAB MKII with an Mg Kα (1253.6 eV) achromatic X-ray source) experiments were performed using the surface analysis system to analyze the elemental composition and binding energies.

The zeta potential and size distribution of nanoparticles (0.05 mg/mL) and dynamic light scattering (DLS) analysis were performed with a Zeta sizer Nano (DLS, Malvern Instruments, Worcestershire, UK). The overall synthesis and preparation mechanism is shown in Scheme 1.

2.8. Catalytic Experimental Method

The catalytic experiments on the decomposition of different dyes were performed in accordance with the previous studies [53,54]. These experiments were conducted outdoors during the daytime (summer) between 12 noon and 2 p.m., on bright and sunny days in Harbin, China (latitude: 45.8038 N, longitude: 126.5350 E). To enhance the intensity of solar light, a convex lens was used to focus it on the reaction mixture.

For the photocatalytic degradation experiment, a Pyrex glass beaker containing a Direct Blue-24 dye sample (0.03 mM) and an appropriate amount of catalyst was placed in a 1000 mL Pyrex glass reservoir outside the laboratory building. The photoreactor, under magnetic stirring, maintained a homogeneous suspension during irradiation, promoting adsorption on the nanocatalyst surface and sunlight absorption. The degraded solution was analyzed at various time intervals after centrifugation at 10,000 rpm for 10 min.

The catalytic efficiency of rGO, rGO–Ag, MXene, and MXene–Ag was examined for the degradation of Direct Blue-24 dye. Changes in the color were observed visually and monitored by UV–Vis spectrophotometry at definite time intervals. Complete degradation of the dye was achieved within a short time for all synthesized products.

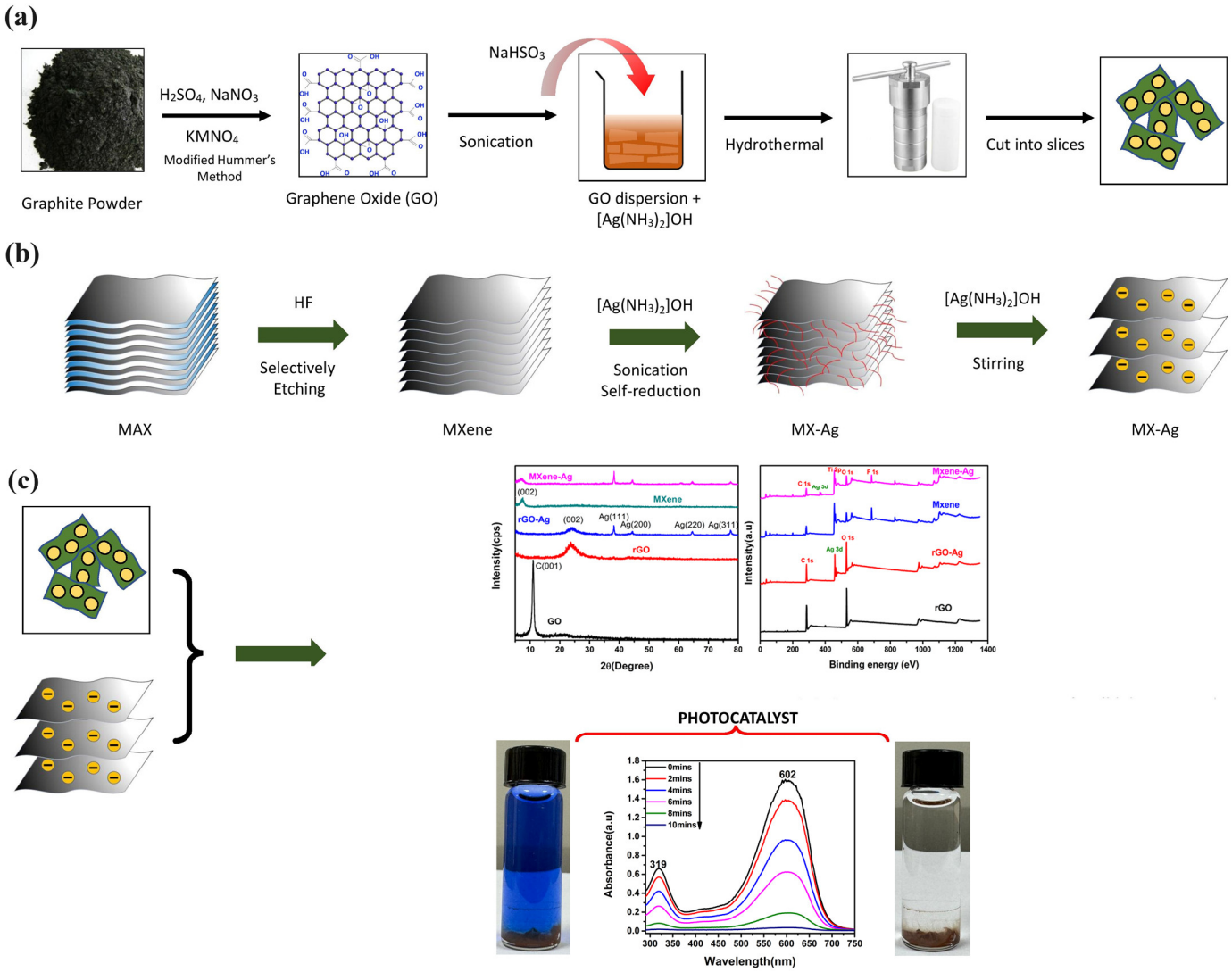

Scheme 1. Preparation mechanism of nanocomposites and their application in dye decomposition: (**a**) represents the preparation process of GO, rGO, and rGO-Ag; (**b**) represents the exfoliation of the MAX phase and the synthesis of MX-Ag nanocomposites; and (**c**) represents the characterization of the prepared nanocomposites and their application in dye decomposition.

3. Result and Discussion

The structure and phase of GO rGO, rGO–Ag, MXene, and MXene–Ag nano composites were characterized using XRD. This confirmed the presence of AgNPs, as shown in Figure 1a. The peaks obtained at approximately 2θ = 8.91°, 10.9°, 24.4°, 38.2°, 44.3°, 64.5°, and 77.6° attributed to the (0 0 1), (0 0 2) crystalline planes of GO, rGO, MXene, rGO–Ag and MXene–Ag. GO exhibited a major peak at the diffraction angle of 10.9° that is attributed to the (0 0 1) reflection plane. After the reduction of GO, the (0 0 1) reflection plane completely vanished, and a new broad diffraction peak appeared at 24.4° that corresponds to the (0 0 2) reflection plane. This shows an increase in the graphitic nature of rGO due to the decreased interlayer spacing, which is also in good correlation with the literature [55]. (0 0 2), (1 1 1), (2 0 0), (2 2 0), and (3 1 1) were the crystalline planes of rGO–Ag, whereas (0 0 2) was the crystalline plane of MXene and (0 0 2), (1 1 1), (2 0 0), (2 2 0), and (3 1 1) were the crystalline planes of MX–Ag nanocomposites, respectively, and the obtained d value of the crystalline plane of the Ag nanocomposite on the (1 1 1) plane was 0.245 nm [10,39]. The crystalline planes of MXene–Ag and rGO–Ag were not measured accurately owing to the decoration of AgNPs that prevented the stacking of the rGO layers [9]. Furthermore, particle size was calculated using the Scherer Equation (1), as mentioned in Table 1 for the MXene–Ag, rGO,

and rGO–Ag composite. After deposition of Ag over MXene and rGO, the peaks due to C1s, N1s, O1s, Ti1s and the Ag3d spectrum can be seen in Figure 1b.

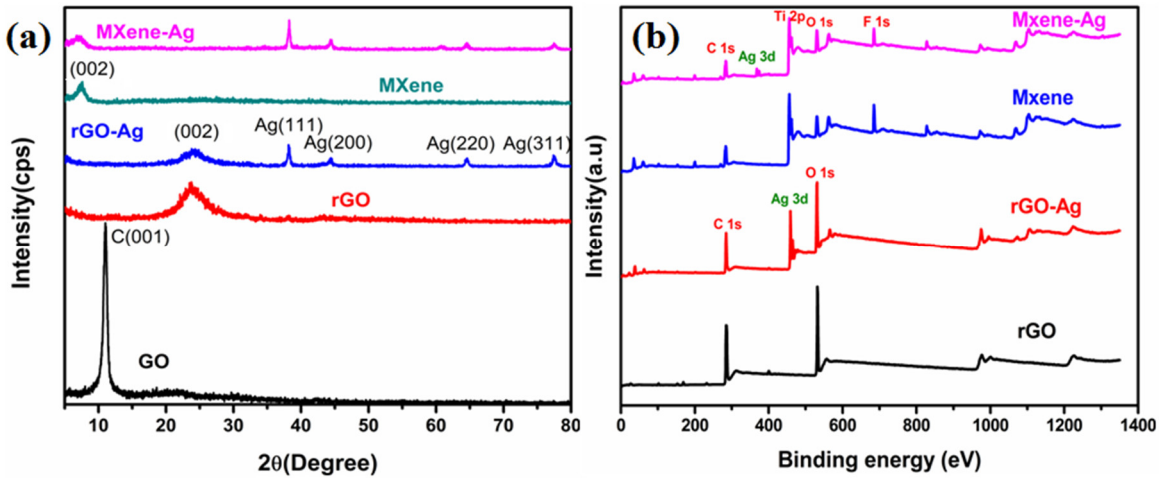

Figure 1. (**a**) XRD pattern of GO, MXene, rGO, rGO–Ag and MXene–Ag nanocomposites, (**b**) XPS pattern of rGO, rGO–Ag, MXene and MX–Ag nanocomposites.

The morphology and chemical characteristics of rGO, rGO–Ag, MXene, and MXene–Ag were measured using TEM. TEM is the most versatile and advanced tool for the measurement of shape, size, chemical constituents, and the exfoliation of the layer-by-layer stacking structure of nano sheets and nano materials. Figures 2 and 3 show the TEM pattern of MXene and MXene–Ag, respectively.

Figure 2a,b shows the different translucent layers of MXene at different magnifications: (a) 500 nm and (b) 1 micrometer. From the Figures, it can be clearly observed that 2D MXene translucent layers were successfully obtained. From these observations, it can be concluded that MXene was prepared from the MAX phase through the selective etching process.

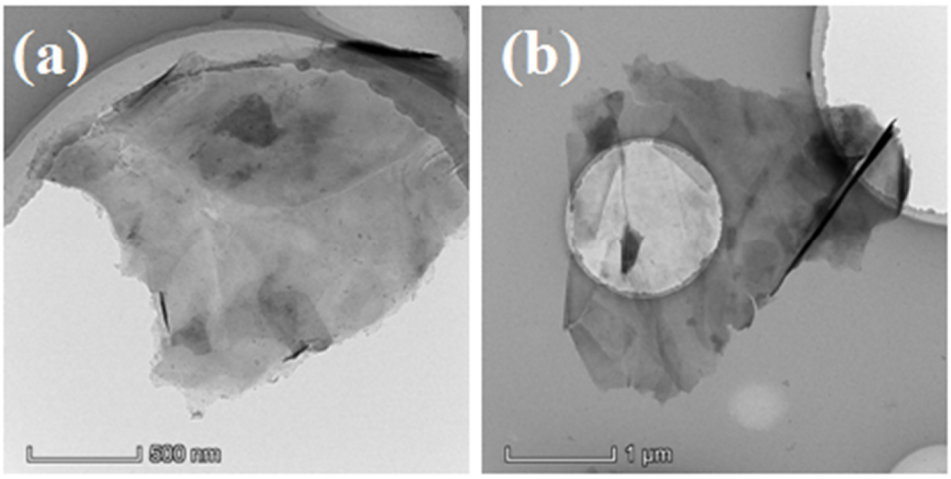

Figure 2. TEM images MXene: (**a**) 500 nm, (**b**) 1 micrometer.

Figure 3a–h show the MXene–Ag nanocomposite: reflected, well dispersed, mainly distributed, and homogenous dispersion with smaller sizes of AgNPs (dark spots) observable on the layers of MXene. The crystallinity of the AgNPs was further investigated by selected-area electron diffraction (SAED). Figure 3 (a-inset graph) shows the typical SAED pattern of the synthesized AgNPs on the MXene nanosheets, which exhibits multiple crystal diffraction features. Two visible diffraction rings can be clearly observed and indexed as face-centered cubic (FCC) metallic silver. The strongest pattern (inner ring) shows the characteristic diffraction rings corresponding to the (111) plane. The outermost ring is

likely attributed to the (311) reflection and confirmed that the AgNPs are in a crystalline nature [39]. The average size of the nanoparticles was 9.62 nm, calculated using nano-measure software (version 1.2), as shown in Figure 6f, which is correlated to AFM as well as the XRD results. Figure 3b–h shows the EDS mapping of each element, and it can be clearly seen that MXene and Ag's nanocomposite was well prepared using the direct reducing method and the elements C, Ag, Fe, O, N, and Ti are present in the nanocomposite.

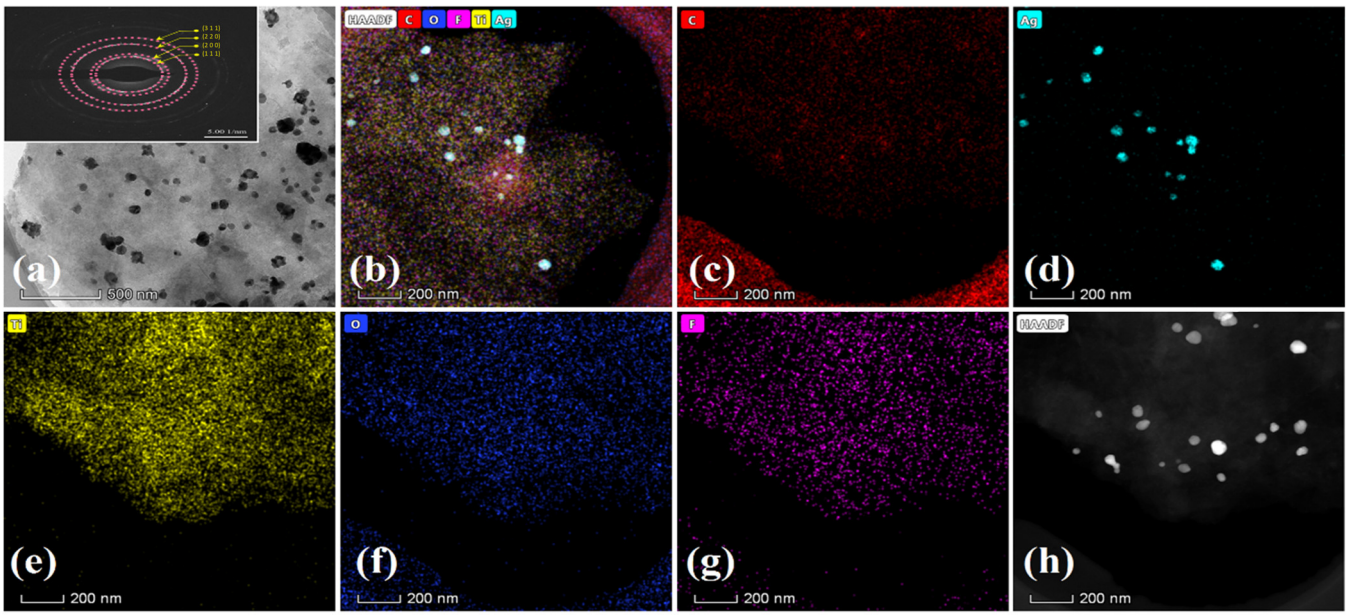

Figure 3. TEM image (**a**), EDS mappings (**b**–**h**) depicting the distribution of elements within the MXene–Ag nanocomposite. The elements C, O, F, Ti, and Ag are discernible in the mappings (**b**) illustrating the presence of C (**c**), focusing on Ag (**d**), (**e**) depicting Ti, (**f**) revealing O, and (**g**) displaying F.

Figure 4a,b show the TEM patterns of the rGO translucent layers on different scales: (a) 200 nm and (b) 500 nm. From the images, it was observed that translucent sheets within the wrinkles and folds of the 2D-reduced Graphene interfere with the oxidation and reduction processes that were successfully achieved using the hydrothermal process.

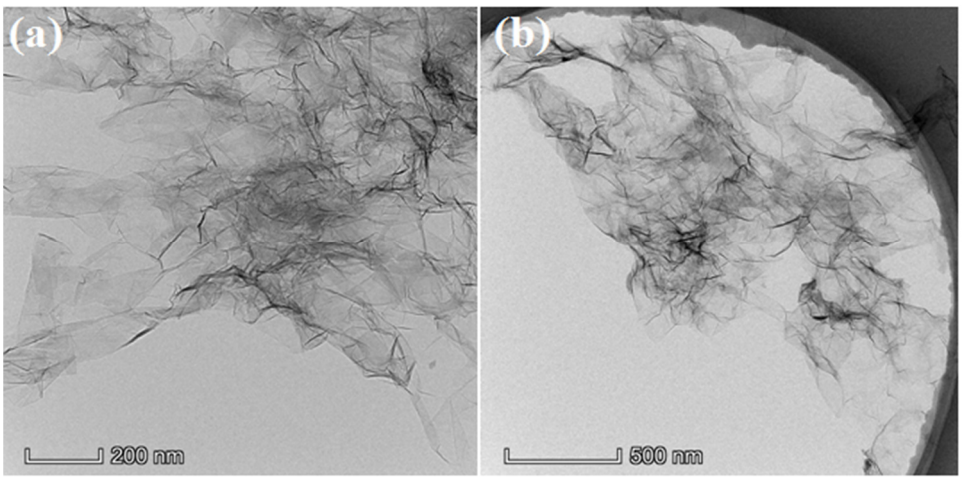

Figure 4. TEM pattern (**a**) 200 nm (**b**) 500 nm of synthesized rGO.

Figure 5a–h shows the TEM pattern, SAED pattern, EDS mapping, and HRTEM of the rGO–Ag composite. Figure 5a presents the mono-dispersed layer of rGO with poly-dispersed decorated Ag spherical nanoparticles attributed to the rGO–Ag nano composite.

It was also confirmed by the appearance of dark patches and spots on the sheet of rGO, which are stabilized/immobilized AgNPs on the rGO layers. The AgNPs are small with an average size of 16.14 nm, as shown in the histogram (Figure 6e), with uniform as well as dense distribution through the rGO layers. The HRTEM (Figure 5h) showed lattice fringes clearly visible with d_{111}0.245 nm, corresponding to the (111) plane [56], which correlated with the XRD pattern. Figure 5b–g show the elemental mapping of the rGO–Ag composite, confirming that elements like C, O, N, and Ag are present in the rGO–Ag composite. Figure 5 (a-inset diagram) shows the typical SAED pattern of synthesized AgNPs on rGO nanosheets, which exhibits poly crystal diffraction features. Different visible diffraction rings can be clearly observed and indexed as face-centered cubic (FCC) metallic silver, indicating that the AgNPs are in a crystalline nature [57].

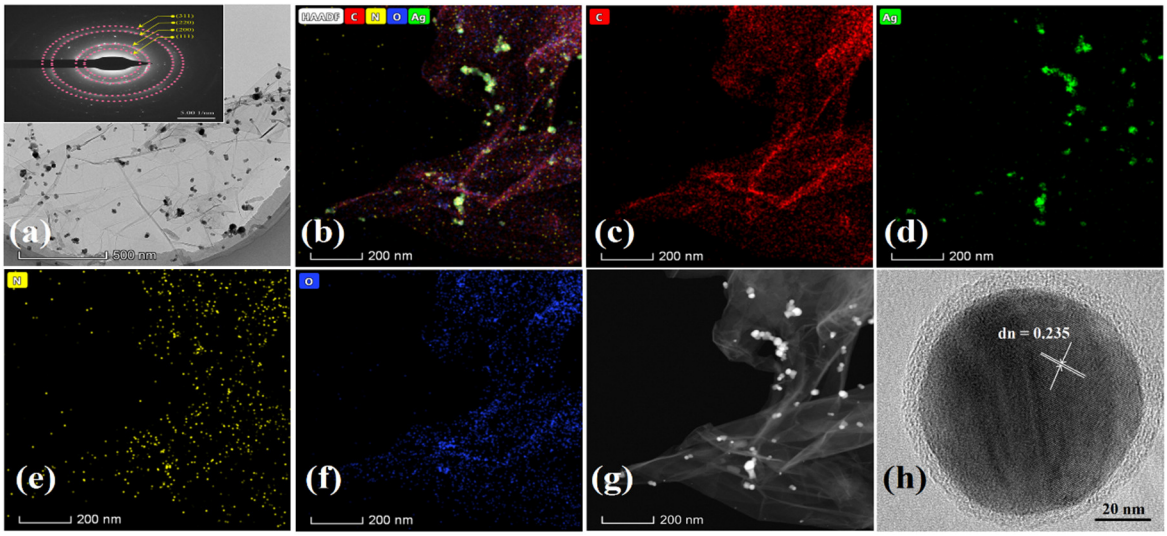

Figure 5. TEM pattern and SAED (inset diagram) (**a**), along with EDS mapping (**b**–**g**) are provided to illustrate the distribution of elements within the synthesized rGO–Ag nanocomposite. The elements C, N, O, and Ag are discernible in the mappings, with (**b**) showing C, N, O, and Ag, (**c**) illustrating C, (**d**) highlighting Ag, (**e**) displaying N, (**f**) revealing O, and (**g**) depicting nanoparticles on the graphene layer. Additionally, (**h**) presents an image of a single crystal of the synthesized rGO–Ag.

According to the characterization of the results obtained from the TEM, it can be observed that MXene and rGO were successfully formed. The obtained results of MXene–Ag and the rGO–Ag nanocomposites showed that the AgNPs had a smaller size and spherical shape with uniform distribution and were successfully formed over the MXene and rGO surface using a $[Ag(NH_3)_2]$ solution, except with $AgNO_3$ alone, as well when using the selective etching and hydrothermal methods. This method also reduced the time for synthesis and also promoted the good dispersion of the NPs. AgNPs can also be prepared with suitable morphology [9,39].

AFM was also performed for the confirmation of the size and shape of the AgNPs composite with rGO and MXene. Figure 6a,c shows the AFM results of the AgNPs (rGO–Ag and MXene–Ag). From these results, it was clearly indicated that the Ag ions were reduced to Ag and AgNPs were successfully obtained in both cases. The surface morphology confirmed that the AgNPs are in a spherical shape and without any aggregation and cracks. The line profile analysis showed the averaged particle size to be 0–40 nm (rGO–Ag) and 0–30 nm (MXene–Ag), as shown in Figure 6b–d and mentioned in Table 2. The data obtained from the AFM analysis correlated well with the XRD and TEM results.

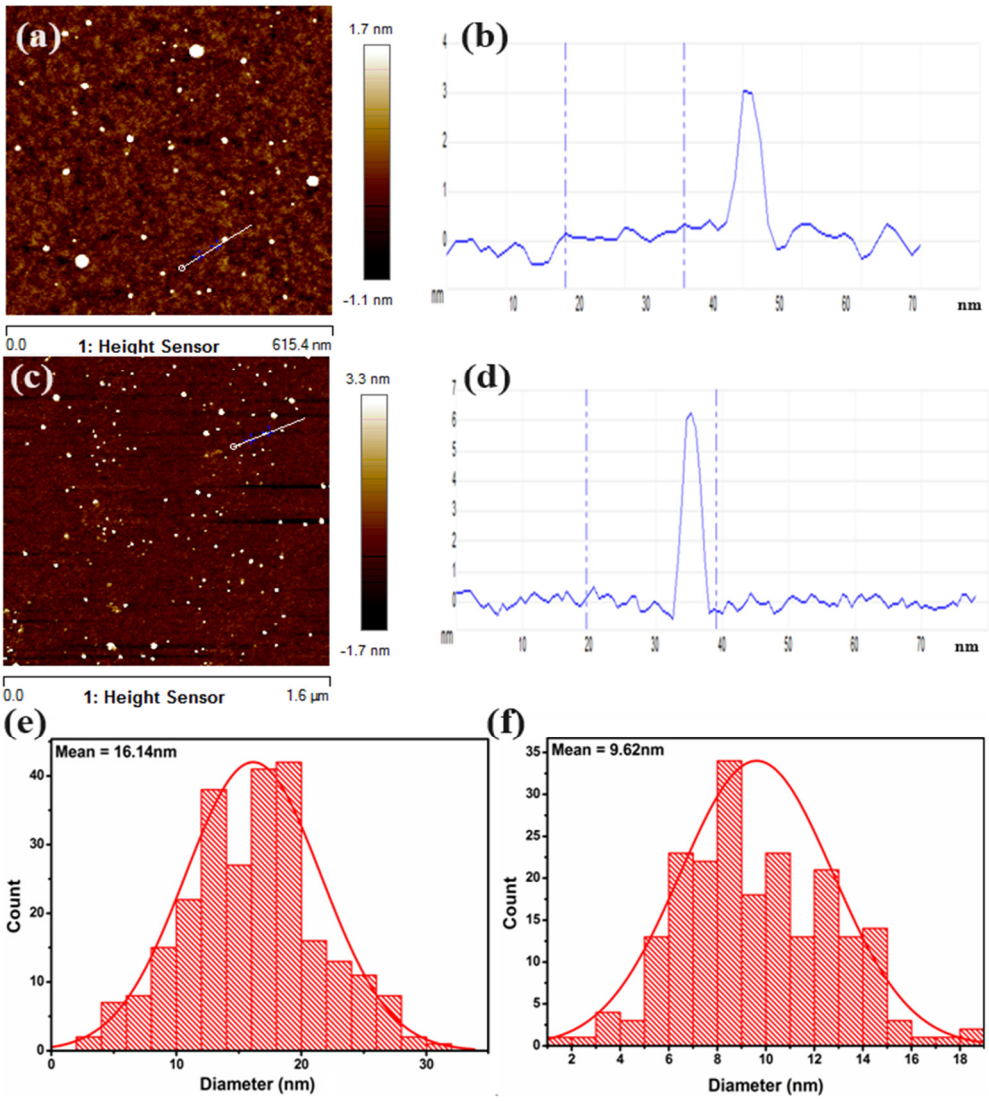

Figure 6. AFM image and line profile of rGO–Ag (**a**,**b**), MX–Ag (**c**,**d**) and histogram of particle size obtained from TEM (**e**) rGO–Ag and (**f**) MX–Ag.

Table 2. Size analysis of synthesized rGO–Ag and MXene–Ag using XRD, AFM, and TEM.

Nanocomposite	XRD			AFM	TEM
	FWHM (Deg)	2θ (Deg)	Size (nm)	Size (nm)	
MX–Ag	0.73214	38.1	11.4	0–30	6.43
rGO–Ag	0.516441	38.2	16.2	0–40	16.14

3.1. Catalytic Activity

3.1.1. Catalytic Mechanism

Photocatalytic activity relies on the interaction between light energy (photons) or wavelength and the catalyst/nanocatalyst. The decomposition of dyes is significantly influenced by $NaBH_4$ and the light source. The literature emphasizes the important role of sunlight in this process. Solar irradiation, or sunlight, impacts electrons within nanoparticles (NPs)/composites, leading to energy absorption and subsequent emission from the valence shell. These highly energetic electrons are instrumental in generating hydroxyl radicals, crucial for degrading dye particles. By utilizing nano catalysts and $NaBH_4$, the nanoparticle acts as an electron relay from the BH_4^- (donor) to the dye (acceptor). BH_4^- ions, known for their nucleophilic nature, interact with the electrophilic dye, transferring

electrons to the NPs. $NaBH_4$ serves as an electron donor and hydrogen provider, while NPs act as electron transfer mediators. Upon adding NPs, reactants (dyes and $NaBH_4$) are simultaneously adsorbed onto the NPs' surface electrostatically. The BH_4^- ion facilitates the transfer of electrons and hydrogen to the azo dyes, resulting in the reductive decomposition of the dyes. The spherical shape of the NPs, along with their high surface-to-volume ratio, provides numerous catalytic sites, reducing the activation energy and facilitating the catalyzed reductive decomposition of dyes [47–53]. Additionally, semiconducting materials function as catalysts, acting as sensitizers for the irradiation of light-induced redox processes. This is attributed to their electron structure, characterized by a vacant conduction band and a filled valence band [58–60].

When a semiconductor is exposed to light-containing photons, and the energy of the incident light matches or exceeds the band gap energy of the semiconductor, electrons in the valence band become energized and transition to the conduction band. This process leaves behind holes in the valence band. These holes can react with donor molecules and water, producing hydroxyl radicals with potent oxidizing capabilities, contributing to pollutant decomposition. Simultaneously, electrons in the conduction band react with dissolved oxygen species, forming superoxide ions, and initiating redox reactions. These electrons and holes can engage in successive oxidation and reduction reactions with any species absorbed on the semiconductor surface, yielding the required end product. The reaction is shown in Figure 7.

It was shown that reaction progress was being made since the NPs were used as a catalytic agent along with $NaBH_4$. Below is a description of what the possible mechanism of the NPs might be.

1. The absorption of photons from solar radiation by the nanoparticles.

$$h_v + NPs/NCs \frac{sunlight}{Solar} h_v^+ + e^- \quad (2)$$

2. Hydrooyle radicals are released as a result of the reaction.

$$h_v^+ \, OH^- \rightarrow OH^- h_v^+ + H_2O + OH^- \quad (3)$$

3. As a result of successful attachment by OH radicals to dye molecules, dye decomposition occurs.

$$\text{dye} + \text{OH}^- \rightarrow \text{Productofdegradtion} + \text{H}_2\text{O} \quad (4)$$

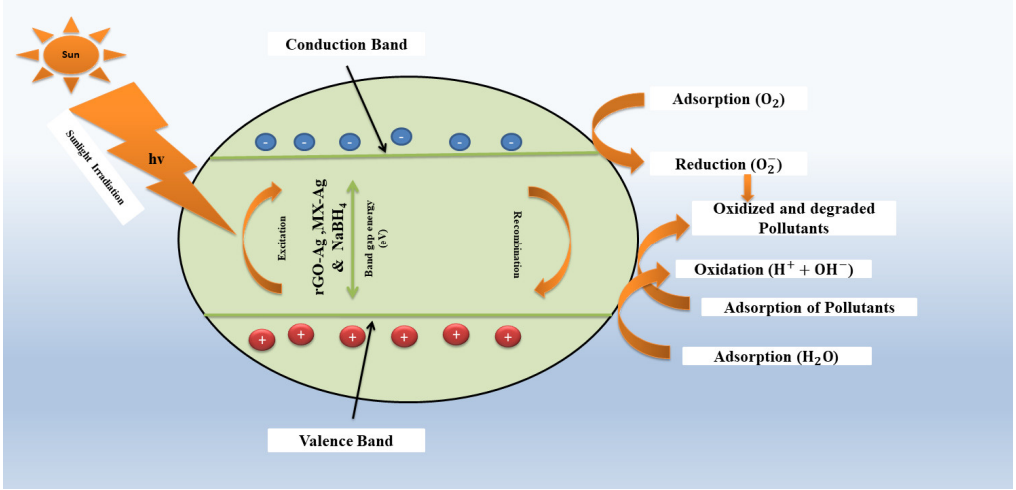

Figure 7. Mechanism of photocatalytic decomposition of dye under solar light, Figure is reproduced with permission from Ref. [61]. 2020, RSC Advances.

3.1.2. Decomposition of Direct Blue-24

All synthesized products (15 mg mL^{-1}) were used for the catalytic decomposition experiments. A DB peak was observed at 319 and 602 nm without NPs and $NaBH_4$ (0.05 mM) [62]. A control experiment was conducted without a catalyst and with $NaBH_4$. A very slow reaction was observed between the components, which may account for the equilibrium state between dye molecules on adsorbent surfaces and the slow decomposition of the DB-24 solution.

The catalytic decomposition was observed using different catalysts till the color changed from blue to colorless. Figure 8a–e shows the UV–Vis spectra of the DB-24 dye at different time intervals during the reaction. There is no doubt that higher color removal was achieved with five minutes of treatment, as the oppositely charged surface was maximized. However, after five minutes, both the absorbance intensity and the rGO–Ag absorbance intensities began to decrease. This may be attributed to the maximum amount of sorption sites being covered by the surface of rGO and rGO–Ag, respectively. For rGO and rGO–Ag, the complete maximum decomposition occurred in 50 and 35 min, respectively, with a very low diffusion rate of dye molecules, which may be explained by the available reactive groups on rGO and rGO–Ag. The dye concentration of DB-24 was kept constant in each of the cases.

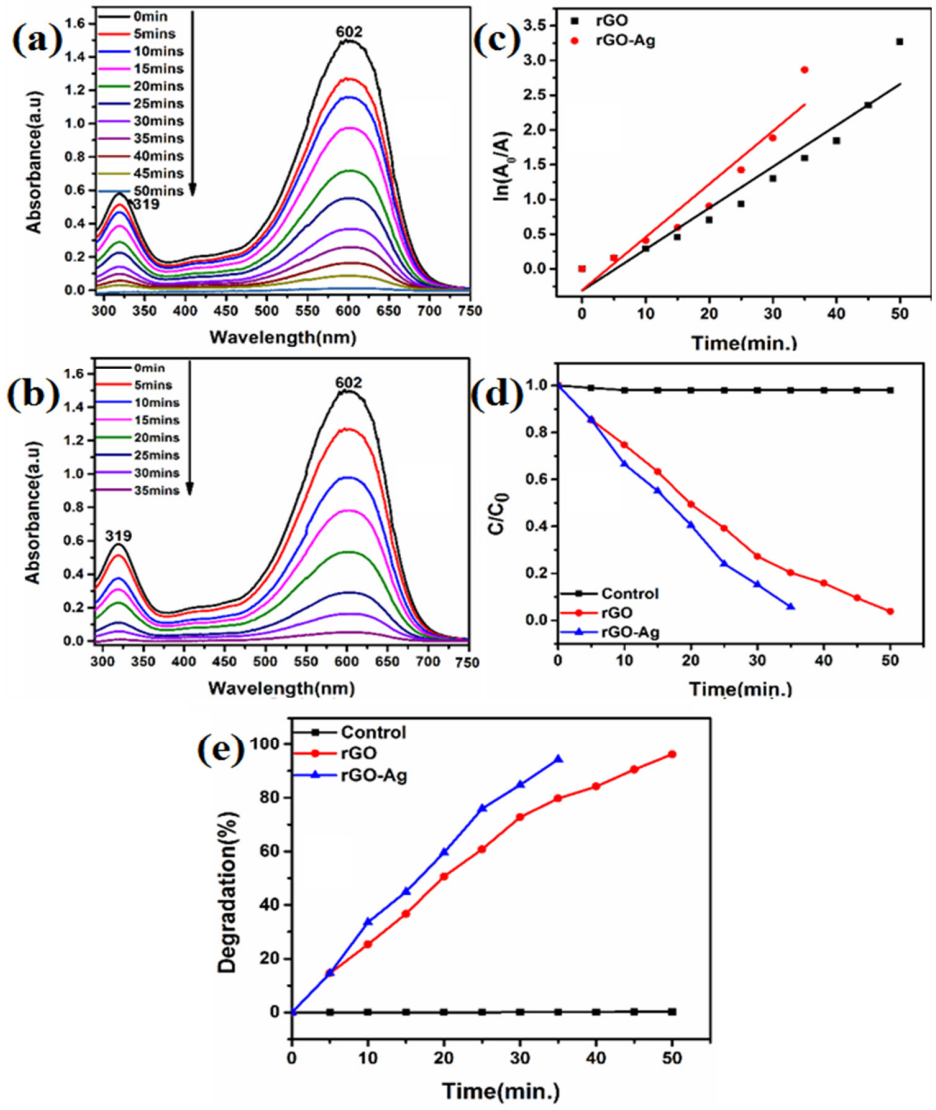

Figure 8. An analysis of the UV–Vis spectral decomposition of DB-24 in the presence of rGO (**a**), rGO–Ag (**b**), linear correlation of ln (A_o/A_t) with time (**c**), concentration decreases with respect to time (**d**) and decomposition % (**e**) of DB-24.

Figure 9a,b UV–Vis spectra were monitored while MXene and MXene–Ag nanocatalysts were observed in sunlight. As a result, complete decomposition was achieved for the MX nanocatalyst and the MXene–Ag nanocatalyst in 16 and 10 min, respectively. A pseudo-first-order reaction kinetic was computed followed by the computation of the rate constant and the R^2 value using the equation: $\ln(A_o/A_t) = kt$. The decomposition efficiencies were calculated using, $D\% = \frac{A_o - A_t}{A_t} \times 100$, at time $t = 0$, A_o represents the initial concentration of the DB-24 solution, and A represents the concentration at time (t). A summary of all the values is shown in Figure 9c,d and in Table 3. Table 3 includes data related to the conversion rates of the nanocatalyst, specifically comparing the catalytic activity of MXene and MXene–Ag with the rGO and rGO–Ag nanocatalysts. MXene and MXene–Ag achieved a higher conversion rate than the rGO and rGO–Ag nanocatalysts. As a result of more catalytic activity of metals than carbon material, the attachment of silver played a vital role in increasing the rate of reaction in both cases. Figure 9c shows the decrease in dye concentration and the degradation % is shown in Figure 9e.

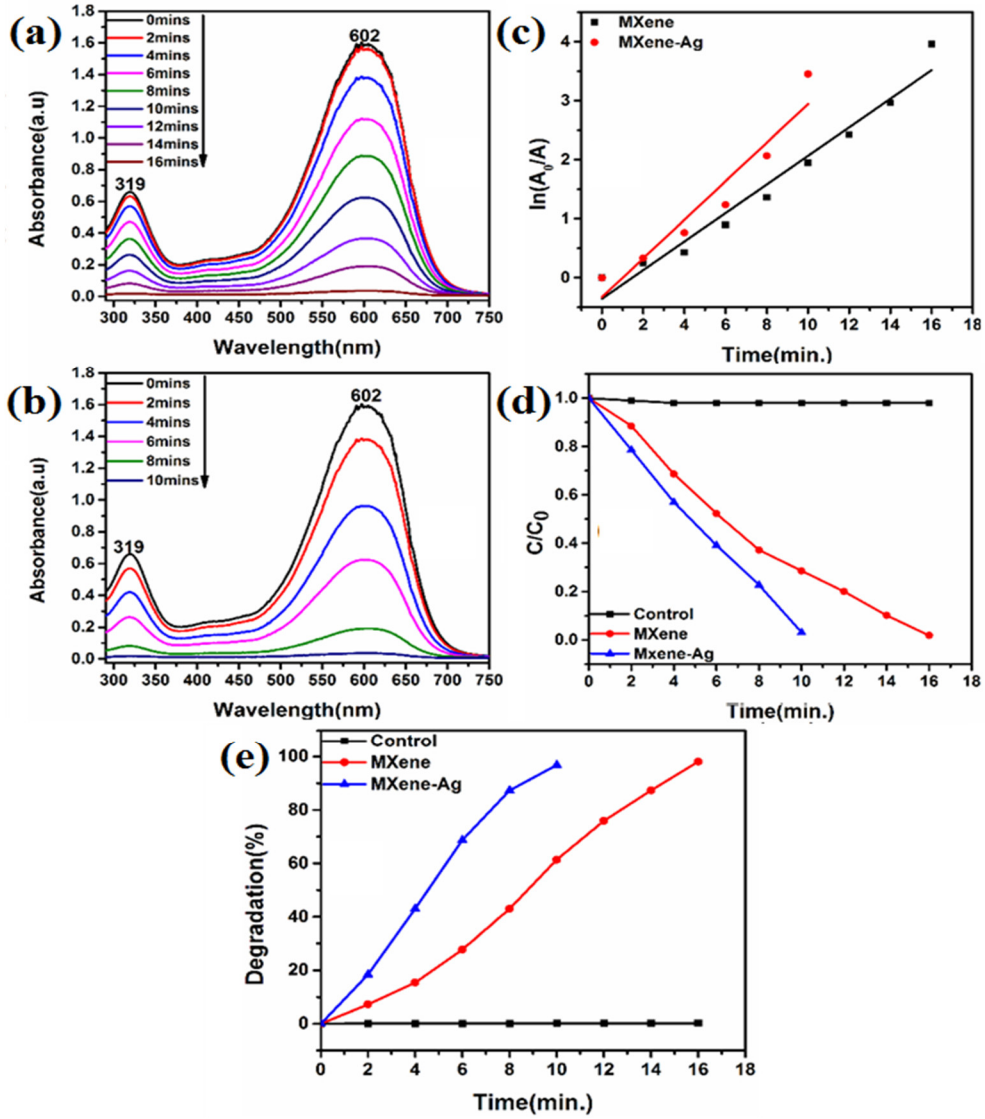

Figure 9. UV–Vis spectral decomposition of DB-24 via catalyst presence MX (**a**), and MX–Ag (**b**), linear correlation of ln (A_o/A_t) with time (**c**), concentration reduction (**d**), decomposition % (**e**) of DB-24.

It was observed that MX–Ag has a greater effect on the decomposition process compared to rGO–Ag. However, maximum decomposition (97–98%) was achieved within 10

to 16 min for the MX and MX–Ag nanocomposites, respectively, as shown in Table 3. The increased performance of MX over rGO can be attributed to the more hydrophilic nature of MX, due to surface terminations of -O, -F, and -OH, and the presence of transition metal carbide/nitride, compared to the hydrophobic characteristics of rGO. MXene is exceptional and is often integrated with other substances in functional composites to enhance its catalytic function in a variety of reactions. With improved thermal stability, electrical conductivity, and electrochemical activity, along with enhanced specific surface structure, MXene can be effectively used in photocatalysis and energy regeneration reactions. Integrating MXene into composite materials further enhances its catalytic performance by improving the specific surface structures and maximizing active sites, particularly in photocatalysis and energy regeneration reactions. A thorough discussion of MXene's role in catalytic enhancement should be considered for its unique properties and synergistic interactions with other components in composite materials, which provides a comprehensive understanding of its catalytic mechanisms and applications [39,63–66].

Table 3. The % RE, rate constants (k) and R^2 values of the linear fit of kinetic plots for the decomposition of DB-24 in addition to the time for achieving the complete decomposition.

Name of Dye	Samples (mg mL^{-1})	Decomposition/Reduction Time (min.)	Decomposition/Reduction Efficiency (%DE)	Rate Constant (k, min^{-1})	R^2
DB-24	rGO	0–50	94	1.0597×10^{-2}	0.924
	rGO–Ag	0–35	96	2.037×10^{-2}	0.903
	MX	0–16	97	2.149×10^{-2}	0.961
	MX–Ag	0–10	98	3.456×10^{-2}	0.924

Additionally, the oxidation of MXene during the preparation of the composites and the photocatalysis process significantly influences their catalytic properties. During the preparation of the composites, oxidation leads to the formation of functional groups on the surface, thereby enhancing its interaction with other materials and improving the stability of the composite. The presence of oxygen-containing functional groups, such as -O, -F, and -OH, on the surface of MXene enhances its hydrophilic nature compared to hydrophobic materials like rGO, resulting in increased catalytic performance [67,68].

In the photocatalysis process, oxidized MXene acts as an efficient catalyst for degrading organic pollutants. The oxygen-containing groups facilitate the generation of reactive oxygen species, such as hydroxyl radicals, essential for pollutant degradation. This oxidation enhances light absorption and charge separation efficiency, leading to more effective pollutant degradation [68,69]. The synergistic interactions between MXene and other components in composite materials play a vital role in enhancing catalytic mechanisms and applications. Therefore, improving the specific surface structures and maximizing the active sites, MXene-based composites exhibit enhanced efficiency in various catalytic applications, particularly in photocatalysis and energy regeneration reactions [69,70].

As shown in Table 4 below, we compared the reduction of different dyes using rGO–Ag and MX–Ag catalysts with those reported in the literature. It can be observed that rGO–Ag and MX–Ag carried out the reduction reaction in the shortest possible time. Additionally, DB-24 dye is rarely used by researchers. Table 4 provides a comparison of various catalysts in the decomposition of different dyes, showcasing the diverse applications and effectiveness of nanocatalysts in tailored catalytic solutions based on specific dye types and reaction conditions. Our study observed that MXene and reduced graphene oxide (rGO) nanocomposites with silver nanoparticles (Ag) exhibited enhanced catalytic activity in degrading Direct Blue-24 dye in a minimal period of time compared to previous studies.

Table 4. Comparison of various catalysts in the decomposition of different kinds of dyes.

S.No.	Materials	Methods	Name of Dyes	Time	Ref.
1	BGFSO/MXene nanohybrids	Co-precipitation	Congo red	120 min	[71]
2	AgNPs	Green synthesis	M.O	24 h	[72]
3	MXene/Cu_2O	Precipitation method	Tetracycline hydrochloride	50 min	[73]
4	AgNPs	Green synthesis	M.O	10 h	[74]
5	AgNPs and TiO_2	Chemical method	M.O	30 min	[75]
6	AgNPs	Green synthesis	C.R	35 min	[76]
7	$BaSnO_3$/Mxene	Electrostatic self assemble	4 Nitrophenol	75 min	[77]
8	Ag and Zn NPs	Chemical method	C.R	50 min	[78]
9	Ag and Au NPs	Green synthesis	C.R	60 min	[79]
10	Cds/Ti_3C_2/TiO_2	Hydrothermal	Methylene blue	150 min	[80]
11	AgNPs	Green synthesis	MO	3 h	[81]
12	$NiFe_2O_4$/Mxene	Ultra-sonification	Methylene blue	70 min	[82]
13	Ag and Au NPs	Green synthesis	C.R	60 min	[83]
14	MXene/$NiMnO_3$/$NiMn_2O_4$	Electrostatic self-assembly method	Rhodamine B, Methylene blue, and methyl orange	50 min	[84]
16	rGO/Fe_3O_4	Facile and eco-friendly co-blending method	Methylene blue,	50 min	[85]
17	Bi_2O_3–rGO	Sono chemical route	Methylene blue,	2 h 40 min, 2 h 20 min and 1 h	[86]
18	CdSe–Graphene	Facile synthesis	Rhodamine B	150 min	[87]
19	MXene–Silver	Chemical method	Safranin dye	15 min	[88]
20	Ag-$LaNiO_3$/MXene	Facile routes	Bromophenol blue, Methyl orange, and benzoic acid	70 min	[89]
21	AgNPs/TiO_2/Ti_3C_2Tx	Hydrothermal method	Methylene blue and Rhodamine B	120 min	[90]
22	MXene-derived Ti_3C_2/TiO_2/Ag	Hydrothermal oxidation method	Oxytetracycline, rhodamine b, methyl orange, and methylene blue	15 min and 45 min	[91]
23	rGO–Ag	Hydrothermal method	Direct Blue-24	35 min	This work
24	MX–Ag	Selective etching and self-reduction method	Direct Blue-24	10 min	This work

4. Reusability and Stability

Ensuring the reusability and recovery of nanocomposites (NCPs) holds paramount importance for practical catalyst applications. Typically, achieving this involves washing the nanocomposites thrice with distilled water, followed by centrifugation. This study investigates the reusability of rGO–AgNPs and MX–Ag in DB-24 reduction. Remarkably, these nanocomposites exhibit sustained performance, retaining their effectiveness for up to five cycles with decomposition rates of 96% and 98%, as illustrated in Figure 10a.

Zeta potential measurements reveal a negative charge of −35.5 mV for rGO–Ag and −38.04 mV for MX–Ag, indicating strong repulsive forces between the NCPs, which enhance their stability and affinity for metal ion fabrication on their surfaces (Figure 10b). Moreover, SEM analysis of the washed and reused nanoparticles (Figure 10c,d) indicates minimal morphological changes even after the fifth cycle. However, prolonged use beyond this point may lead to nanoparticle poisoning and reduced decomposition efficiency [88,92,93].

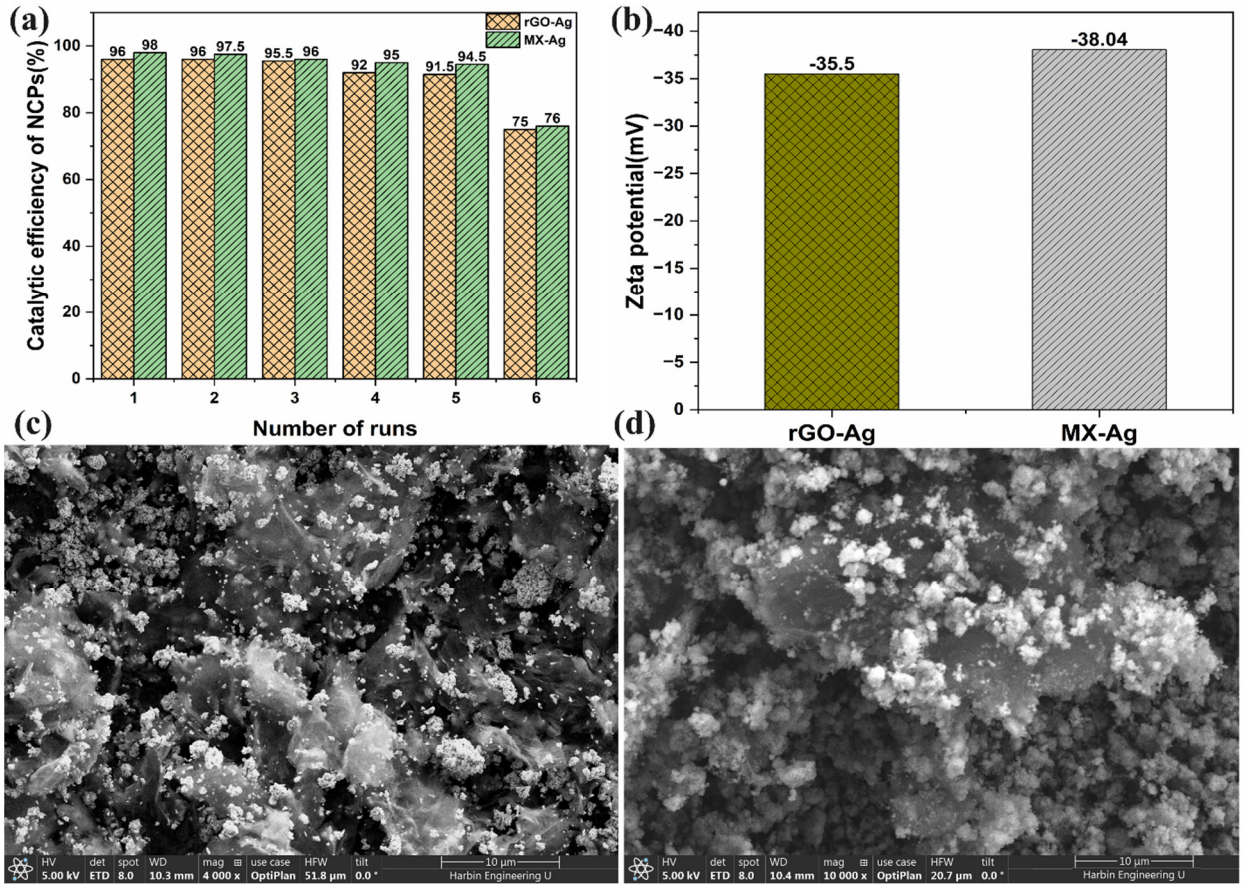

Figure 10. Decomposition (%) as shown in column graph (**a**), Zeta potential (**b**), SEM images of rGO–Ag (**c**) and MX–Ag (**d**).

5. Conclusions

In this work, Graphene oxide (GO) was prepared using the modified Hummer's method and MXene was produced by selectively etching the MAX phase into a hydrofluoric acid solution. MXene–silver nanoparticles (MXene–Ag) were synthesized using the direct reduction method with an ammoniacal solution (aqueous solution). A nanocomposite based on reduced GO–Silver (rGO–Ag) nanoparticles was prepared using the hydrothermal method. Highly concentrated, small, and uniformly dispersed Ag-based composites presented a large surface area of the functional active sites for improved photocatalytic activity. These nanocomposites were evaluated morphologically and chemically using XRD, TEM, HRTEM, EDS mapping, AFM, and XPS. According to the XRD, TEM and AFM results, the average particle size of the AgNPs observed in the rGO–Ag sheet was ~20 nm while in the MXene–Ag sheet was ~10 nm. Characterization results from XRD, TEM, HRTEM, EDS mapping, AFM, and XPS confirmed the successful formation of MXene and rGO. The MXene–Ag and rGO–Ag nanocomposites showed that the AgNPs had a smaller size and spherical shape with uniform distribution, successfully formed on the MXene and rGO surfaces using a $[Ag(NH_3)_2]$ solution as well as $AgNO_3$ alone, by selective etching and hydrothermal methods. This method also reduced the synthesis time and promoted good dispersion of the NPs. Both synthesized composites showed successful degradation of Direct Blue-24 dye. However, it was found that MX–Ag exhibited a greater impact on the degradation process compared to rGO–Ag. Notably, the maximum degradation, i.e., 97–98%, occurred within 10 to 16 min for MX and MX–Ag nanocomposites, while rGO and rGO–Ag nanocatalysts achieved 94–96% degradation in 35 to 50 min. Hence, the methods of preparing MXene–Ag and rGO–Ag nanocomposites can be considered to obtain various types of MXene and rGO-based metallic nanocomposites for more useful and advanced

fields. The results of this research may find a useful application for treating various types of industrial wastewater at a commercial level.

6. Drawback of the Study and Future Scope

This study demonstrated the enhanced catalytic efficiency of Ag-attached MXene nanocomposites for dye decomposition. Specific limitations can be attributed to the selection of a specific dye (Direct Blue-24). Future research could explore the catalytic performance of these synthesized nanocomposites for a broader range of dye stuffs and concentrations. Additionally, investigating the stability and recyclability of synthesized products under various environmental conditions would also provide valuable insights for more diverse practical applications.

Author Contributions: Conceptualization, K.C.; methodology, K.C.; software, M.A. and M.J.A.; validation, A.H.S. and K.C.; formal analysis, M.A. and A.H.S.; investigation, K.C.; resources, K.C.; data curation, M.N.L. and M.M.A.; writing—original draft preparation, K.C. and A.H.S.; writing—review and editing, K.C., M.M.A., M.N.L., M.J.A. and A.H.S.; visualization, M.A.; supervision, K.C.; project administration, K.C.; funding acquisition, K.C. All authors have read and agreed to the published version of the manuscript.

Funding: The research work was funded by the National Natural Science Foundation of China and Harbin Engineering University, China.

Data Availability Statement: Data are contained within the article.

Conflicts of Interest: The authors declare no conflicts of interest.

References

1. Ding, X.; Li, C.; Wang, L.; Feng, L.; Han, D.; Wang, W. Fabrication of hierarchical g-C_3N_4/MXene-AgNPs nanocomposites with enhanced photocatalytic performances. *Mater. Lett.* **2019**, *247*, 174–177. [CrossRef]
2. Xin, W.; Xi, G.-Q.; Cao, W.-T.; Ma, C.; Liu, T.; Ma, M.-G.; Bian, J. Lightweight and flexible MXene/CNF/silver composite membranes with a brick-like structure and high-performance electromagnetic-interference shielding. *RSC Adv.* **2019**, *9*, 29636–29644. [CrossRef]
3. Meng, N.; Zhang, S.; Zhou, Y.; Nie, W.; Chen, P. Novel synthesis of silver/reduced graphene oxide nanocomposite and its high catalytic activity towards hydrogenation of 4-nitrophenol. *RSC Adv.* **2015**, *5*, 70968–70971. [CrossRef]
4. Lv, Z.; Wu, Y.; Lin, J.; Li, W.; Weisbecker, H.; Wang, P.; Song, X.; Sun, W.; Sun, Z.; Xie, Y.; et al. Schottky Heterojunction Facilitates Osteosarcoma Ferroptosis and Enhances Bone Formation in a Switchable Mode. *Adv. Funct. Mater.* **2024**, *34*, 2312032. [CrossRef]
5. Kahrilas, G.A.; Haggren, W.; Read, R.L.; Wally, L.M.; Fredrick, S.J.; Hiskey, M.; Prieto, A.L.; Owens, J.E. Investigation of Antibacterial Activity by Silver Nanoparticles Prepared by Microwave-Assisted Green Syntheses with Soluble Starch, Dextrose, and Arabinose. *ACS Sustain. Chem. Eng.* **2014**, *2*, 590–598. [CrossRef]
6. Deepi, A.; Srikesh, G.; Nesaraj, A.S. One pot reflux synthesis of reduced graphene oxide decorated with silver/cobalt oxide: A novel nano composite material for high capacitance applications. *Ceram. Int.* **2018**, *44*, 20524–20530. [CrossRef]
7. Xia, B.; He, F.; Li, L. Preparation of bimetallic nanoparticles using a facile green synthesis method and their application. *Langmuir* **2013**, *29*, 4901–4907. [CrossRef]
8. Pu, F.; Huang, Y.; Yang, Z.; Qiu, H.; Ren, J. Nucleotide-Based Assemblies for Green Synthesis of Silver Nanoparticles with Controlled Localized Surface Plasmon Resonances and Their Applications. *ACS Appl. Mater. Interfaces* **2018**, *10*, 9929–9937. [CrossRef]
9. Zhao, R.; Kong, W.; Sun, M.; Yang, Y.; Liu, W.; Lv, M.; Song, S.; Wang, L.; Song, H.; Hao, R. Highly Stable Graphene-Based Nanocomposite (GO-PEI-Ag) with Broad-Spectrum, Long-Term Antimicrobial Activity and Antibiofilm Effects. *ACS Appl. Mater. Interfaces* **2018**, *10*, 17617–17629. [CrossRef]
10. Minh Dat, N.; Linh, V.N.P.; Huy, L.A.; Huong, N.T.; Tu, T.H.; Phuong, N.T.L.; Nam, H.M.; Thanh Phong, M.; Hieu, N.H. Fabrication and antibacterial activity against Pseudomonas aeruginosa and Staphylococcus aureus of silver nanoparticle decorated reduced graphene oxide nanocomposites. *Mater. Technol.* **2019**, *34*, 369–375. [CrossRef]
11. Kumar, P.; Huo, P.; Zhang, R.; Liu, B. Antibacterial Properties of Graphene-Based Nanomaterials. *Nanomater* **2019**, *9*, 737. [CrossRef] [PubMed]
12. Zhang, H.; Wang, X.; Li, Y.; Guo, C.; Zhang, C. Preparation and characterization of silver-doped graphene-reinforced silver matrix bulk composite as a novel electrical contact material. *Appl. Phys. A* **2019**, *125*, 86. [CrossRef]
13. Jose, P.P.A.; Kala, M.S.; Kalarikkal, N.; Thomas, S. Reduced graphene oxide produced by chemical and hydrothermal methods. *Mater. Today Proc.* **2018**, *5*, 16306–16312. [CrossRef]

14. Nguyen, M.D.; Pham, V.D.K.; Nguyen, L.P.T.; Hoang, M.N.; Nguyen, H.H. Synthesis and antibacterial activity of silver/reduced graphene oxide nanocomposites against Salmonella typhimurium and Staphylococcus aureus. *Nanosci. Nanotechnol.* **2018**, *60*, 67–73. [CrossRef] [PubMed]
15. Li, H.; Du, Z. Preparation of a Highly Sensitive and Stretchable Strain Sensor of MXene/Silver Nanocomposite-Based Yarn and Wearable Applications. *ACS Appl. Mater. Interfaces* **2019**, *11*, 45930–45938. [CrossRef] [PubMed]
16. Liu, S.; Zeng, T.H.; Hofmann, M.; Burcombe, E.; Wei, J.; Jiang, R.; Kong, J.; Chen, Y. Antibacterial Activity of Graphite, Graphite Oxide, Graphene Oxide, and Reduced Graphene Oxide: Membrane and Oxidative Stress. *Am. Chem. Soc.* **2011**, *5*, 6971–6980. [CrossRef] [PubMed]
17. Zou, X.; Zhang, L.; Wang, Z.; Luo, Y. Mechanisms of the Antimicrobial Activities of Graphene Materials. *J. Am. Chem. Soc.* **2016**, *138*, 2064–2077. [CrossRef]
18. Koushik, D.; Sen Gupta, S.; Maliyekkal, S.M.; Pradeep, T. Rapid dehalogenation of pesticides and organics at the interface of reduced graphene oxide-silver nanocomposite. *J. Hazard. Mater.* **2016**, *308*, 192–198. [CrossRef]
19. Lawal, A.T. Graphene-based nano composites and their applications. A review. *Biosens. Bioelectron.* **2019**, *141*, 111384. [CrossRef] [PubMed]
20. Ponja, S.D.; Sehmi, S.K.; Allan, E.; MacRobert, A.J.; Parkin, I.P.; Carmalt, C.J. Enhanced Bactericidal Activity of Silver Thin Films Deposited via Aerosol-Assisted Chemical Vapor Deposition. *ACS Appl. Mater. Interfaces* **2015**, *7*, 28616–28623. [CrossRef]
21. Jaworski, S.; Wierzbicki, M.; Sawosz, E.; Jung, A.; Gielerak, G.; Biernat, J.; Jaremek, H.; Lojkowski, W.; Wozniak, B.; Wojnarowicz, J.; et al. Graphene Oxide-Based Nanocomposites Decorated with Silver Nanoparticles as an Antibacterial Agent. *Nanoscale Res. Lett.* **2018**, *13*, 116. [CrossRef]
22. Quezada-Renteria, J.A.; Chazaro-Ruiz, L.F.; Rangel-Mendez, J.R. Poorly conductive electrochemically reduced graphene oxide films modified with alkyne chains to avoid the corrosion-promoting effect of graphene-based materials on carbon steel. *Carbon* **2020**, *167*, 512–522. [CrossRef]
23. Sims, C.M.; Hanna, S.K.; Heller, D.A.; Horoszko, C.P.; Johnson, M.E.; Montoro Bustos, A.R.; Reipa, V.; Riley, K.R.; Nelson, B.C. Redox-active nanomaterials for nanomedicine applications. *Nanoscale* **2017**, *9*, 15226–15251. [CrossRef]
24. Szunerits, S.; Boukherroub, R. Antibacterial activity of graphene-based materials. *J. Mater. Chem. B* **2016**, *4*, 6892–6912. [CrossRef]
25. Cui, Y.; Yang, K.; Wang, J.; Shah, T.; Zhang, Q.; Zhang, B. Preparation of pleated rGO/MXene/Fe_3O_4 microsphere and its absorption properties for electromagnetic wave. *Carbon* **2021**, *172*, 1–14. [CrossRef]
26. Galpaya, D.; Wang, M.; Liu, M.; Motta, N.; Waclawik, E.; Yan, C. Recent Advances in Fabrication and Characterization of Graphene-Polymer Nanocomposites. *Graphene* **2012**, *1*, 30–49. [CrossRef]
27. Stankovich, S.; Dikin, D.A.; Piner, R.D.; Kohlhaas, K.A.; Kleinhammes, A.; Jia, Y.; Wu, Y.; Nguyen, S.T.; Ruoff, R.S. Synthesis of graphene-based nanosheets via chemical reduction of exfoliated graphite oxide. *Carbon* **2007**, *45*, 1558–1565. [CrossRef]
28. Zhang, J.; Yang, H.; Shen, G.; Cheng, P.; Zhang, J.; Guo, S. Reduction of graphene oxide via L-ascorbic acid. *Chem. Commun.* **2010**, *46*, 1112–1114. [CrossRef]
29. Mao, S.; Yu, K.; Cui, S.; Bo, Z.; Lu, G.; Chen, J. A new reducing agent to prepare single-layer, high-quality reduced graphene oxide for device applications. *Nanoscale* **2011**, *3*, 2849–2853. [CrossRef]
30. Bo, Z.; Shuai, X.; Mao, S.; Yang, H.; Qian, J.; Chen, J.; Yan, J.; Cen, K. Green preparation of reduced graphene oxide for sensing and energy storage applications. *Sci. Rep.* **2014**, *4*, 4684. [CrossRef]
31. Egorova, M.N.; Tarasova, L.A.; Vasilieva, F.D.; Akhremenko, Y.A.; Smagulova, S.A. Antimicrobial activity of graphene oxide sheets. In Proceedings of the 6th International Conference on Production, Energy and Reliability 2018: World Engineering Science & Technology Congress (ESTCON), Kuala Lumpur, Malaysia, 13–14 August 2018.
32. Zhang, X.; Zhang, J.; Chen, Y.; Cheng, K.; Yan, J.; Zhu, K.; Ye, K.; Wang, G.; Zhou, L.; Cao, D. Freestanding 3D Polypyrrole@reduced graphene oxide hydrogels as binder-free electrode materials for flexible asymmetric supercapacitors. *J. Colloid Interface Sci.* **2019**, *536*, 291–299. [CrossRef]
33. Sahu, S.K.; Boggarapu, V.; Sreekanth, P.S.R. Improvements in the mechanical and thermal characteristics of polymer matrix composites reinforced with various nanofillers: A brief review. *Mater. Today Proc.* 2023, in press. [CrossRef]
34. Pan, F.; Yu, L.; Xiang, Z.; Liu, Z.; Deng, B.; Cui, E.; Shi, Z.; Li, X.; Lu, W. Improved synergistic effect for achieving ultrathin microwave absorber of 1D Co nanochains/2D carbide MXene nanocomposite. *Carbon* **2021**, *172*, 506–515. [CrossRef]
35. Chen, M.; Hu, X.; Li, K.; Sun, J.; Liu, Z.; An, B.; Zhou, X.; Liu, Z. Self-assembly of dendritic-lamellar MXene/Carbon nanotube conductive films for wearable tactile sensors and artificial skin. *Carbon* **2020**, *164*, 111–120. [CrossRef]
36. Wu, Y.; Yang, D.; Zhang, Y.; Jiao, S.; Tang, W.; Wang, Z.; Wu, N.; Wang, Y.; Zhong, W.; Zhang, A.; et al. Integrated unit-cell-thin MXene and Schottky electric field into piezo-photocatalyst for enhanced photocarrier separation and hydrogen evolution. *Chem. Eng. J.* **2022**, *439*, 135640. [CrossRef]
37. Gogotsi, Y.; Anasori, B. The Rise of MXenes. *ACS Nano* **2019**, *13*, 8491–8494. [CrossRef]
38. Wu, Y.; Song, X.; Zhou, X.; Song, R.; Tang, W.; Yang, D.; Wang, Y.; Lv, Z.; Zhong, W.; Cai, H.-L.; et al. Piezo-Activated Atomic-Thin Molybdenum Disulfide/MXene Nanoenzyme for Integrated and Efficient Tumor Therapy via Ultrasound-Triggered Schottky Electric Field. *Small* **2023**, *19*, 2205053. [CrossRef]
39. Zou, G.; Zhang, Z.; Guo, J.; Liu, B.; Zhang, Q.; Fernandez, C.; Peng, Q. Synthesis of MXene/Ag Composites for Extraordinary Long Cycle Lifetime Lithium Storage at High Rates. *ACS Appl. Mater. Interfaces* **2016**, *8*, 22280–22286. [CrossRef]
40. Carey, M.; Barsoum, M.W. MXene polymer nanocomposites: A review. *Mater. Today Adv.* **2021**, *9*, 100120. [CrossRef]

41. Rasool, K.; Pandey, R.P.; Rasheed, P.A.; Buczek, S.; Gogotsi, Y.; Mahmoud, K.A. Water treatment and environmental remediation applications of two-dimensional metal carbides (MXenes). *Mater. Today* **2019**, *30*, 80–102. [CrossRef]
42. Huang, X.; Wang, R.; Jiao, T.; Zou, G.; Zhan, F.; Yin, J.; Zhang, L.; Zhou, J.; Peng, Q. Facile Preparation of Hierarchical AgNP-Loaded MXene/Fe_3O_4/Polymer Nanocomposites by Electrospinning with Enhanced Catalytic Performance for Wastewater Treatment. *ACS Omega* **2019**, *4*, 1897–1906. [CrossRef]
43. Chaudhari, N.K.; Jin, H.; Kim, B.; San Baek, D.; Joo, S.H.; Lee, K. MXene: An emerging two-dimensional material for future energy conversion and storage applications. *J. Mater. Chem. A* **2017**, *5*, 24564–24579. [CrossRef]
44. Chand, K.; Zhang, X.; Chen, Y. Recent progress in MXene and graphene based nanocomposites for microwave absorption and electromagnetic interference shielding. *Arab. J. Chem.* **2022**, *15*, 104143. [CrossRef]
45. Azeem, M.M.; Shafa, M.; Aamir, M.; Zubair, M.; Souayeh, B.; Alam, M.W. Nucleotide detection mechanism and comparison based on low-dimensional materials: A review. *Front. Bioeng. Biotechnol.* **2023**, *11*, 1117871. [CrossRef]
46. Sangili, A.; Annalakshmi, M.; Chen, S.-M.; Balasubramanian, P.; Sundrarajan, M. Synthesis of silver nanoparticles decorated on core-shell structured tannic acid-coated iron oxide nanospheres for excellent electrochemical detection and efficient catalytic reduction of hazardous 4-nitrophenol. *Compos. Part B Eng.* **2019**, *162*, 33–42. [CrossRef]
47. Chen, X.; Liang, Y.; Wan, L.; Xie, Z.; Easton, C.D.; Bourgeois, L.; Wang, Z.; Bao, Q.; Zhu, Y.; Tao, S.; et al. Construction of porous N-doped graphene layer for efficient oxygen reduction reaction. *Chem. Eng. Sci.* **2019**, *194*, 36–44. [CrossRef]
48. Ocsoy, I.; Paret, M.L.; Ocsoy, M.A.; Kunwar, S.; Chen, T.; You, M.; Tan, W. Nanotechnology in Plant Disease Management: DNA-Directed Silver Nanoparticles on Graphene Oxide as an Antibacterial against Xanthomonas perforans. *Am. Chem. Soc.* **2013**, *7*, 8972–8980. [CrossRef] [PubMed]
49. Xu, D.; Ma, K.; Chen, L.; Hu, Y.; Jiang, H.; Li, C. MXene interlayer anchored Fe_3O_4 nanocrystals for ultrafast Li-ion batteries. *Chem. Eng. Sci.* **2020**, *212*, 115342. [CrossRef]
50. Zhai, L.-F.; Kong, S.-Y.; Zhang, H.; Tian, W.; Sun, M.; Sun, H.; Wang, S. Facile synthesis of Co-N-rGO composites as an excellent electrocatalyst for oxygen reduction reaction. *Chem. Eng. Sci.* **2019**, *194*, 45–53. [CrossRef]
51. Li, K.; Jiao, T.; Xing, R.; Zou, G.; Zhou, J.; Zhang, L.; Peng, Q. Fabrication of tunable hierarchical MXene@AuNPs nanocomposites constructed by self-reduction reactions with enhanced catalytic performances. *Sci. China Mater.* **2018**, *61*, 728–736. [CrossRef]
52. Sher Shah, M.S.; Park, A.R.; Zhang, K.; Park, J.H.; Yoo, P.J. Green synthesis of biphasic TiO_2-reduced graphene oxide nanocomposites with highly enhanced photocatalytic activity. *ACS Appl. Mater. Interfaces* **2012**, *4*, 3893–3901. [CrossRef] [PubMed]
53. Shyamala, R.; Gomathi Devi, L. Reduced graphene oxide/SnO_2 nanocomposites for the photocatalytic degradation of rhodamine B: Preparation, characterization, photosensitization, vectorial charge transfer mechanism and identification of reaction intermediates. *Chem. Phys. Lett.* **2020**, *748*, 137385. [CrossRef]
54. Gomathi Devi, L.; Shyamala, R. Photocatalytic activity of SnO_2–α-Fe_2O_3 composite mixtures: Exploration of number of active sites, turnover number and turnover frequency. *Mater. Chem. Front.* **2018**, *2*, 796–806. [CrossRef]
55. Kumar, A.; Sadanandhan, A.M.; Jain, S.L. Silver doped reduced graphene oxide as a promising plasmonic photocatalyst for oxidative coupling of benzylamines under visible light irradiation. *New J. Chem.* **2019**, *43*, 9116–9122. [CrossRef]
56. Beiranvand, M.; Farhadi, S.; Mohammadi, A. Graphene Oxide/Hydroxyapatite/Silver (rGO/HAP/Ag) nanocomposite: Synthesis, characterization, catalytic and antibacterial activity. *Int. J. Nano Dimens.* **2019**, *10*, 180–194.
57. Zhang, W.; Li, Z.; Gu, H.; Li, Y.; Zhang, G.; Zhang, F.; Fan, X. l-proline covalently anchored on graphene oxide as an effective bifunctional catalyst for ketene forming reaction. *Chem. Eng. Sci.* **2015**, *135*, 187–192. [CrossRef]
58. Saravanan, R.; Gracia, F.; Stephen, A. Basic Principles, Mechanism, and Challenges of Photocatalysis. In *Nanocomposites for Visible Light-Induced Photocatalysis*; Springer Series on Polymer and Composite Materials; Springer: Berlin/Heidelberg, Germany, 2017; pp. 19–40.
59. Vanaamudan, A.; Soni, H.; Padmaja Sudhakar, P. Palm shell extract capped silver nanoparticles—As efficient catalysts for degradation of dyes and as SERS substrates. *J. Mol. Liq.* **2016**, *215*, 787–794. [CrossRef]
60. Chand, K.; Cao, D.; Eldin Fouad, D.; Hussain Shah, A.; Qadeer Dayo, A.; Zhu, K.; Nazim Lakhan, M.; Mehdi, G.; Dong, S. Green synthesis, characterization and photocatalytic application of silver nanoparticles synthesized by various plant extracts. *Arab. J. Chem.* **2020**, *13*, 8248–8261. [CrossRef]
61. Chen, Y.; Xiang, Z.; Wang, D.; Kang, J.; Qi, H. Effective photocatalytic degradation and physical adsorption of methylene blue using cellulose/GO/TiO_2 hydrogels. *RSC Adv.* **2020**, *10*, 23936–23943. [CrossRef] [PubMed]
62. Bogireddy, N.K.R.; Kiran Kumar, H.A.; Mandal, B.K. Biofabricated silver nanoparticles as green catalyst in the degradation of different textile dyes. *J. Environ. Chem. Eng.* **2016**, *4*, 56–64. [CrossRef]
63. Li, L.; Zhang, N.; Zhang, M.; Wu, L.; Zhang, X.; Zhang, Z. Ag-Nanoparticle-Decorated 2D Titanium Carbide (MXene) with Superior Electrochemical Performance for Supercapacitors. *ACS Sustain. Chem. Eng.* **2018**, *6*, 7442–7450. [CrossRef]
64. Rasool, K.; Helal, M.; Ali, A.; Ren, C.E.; Gogotsi, Y.; Mahmoud, K.A. Antibacterial Activity of $Ti_3C_2T_x$ MXene. *ACS Nano* **2016**, *10*, 3674–3684. [CrossRef] [PubMed]
65. Wu, X.; Wang, Y.; Wu, Z.S. Recent advancement and key opportunities of MXenes for electrocatalysis. *iScience* **2024**, *27*, 108906. [CrossRef]
66. Sun, Z.; Wang, R.; Matulis, V.E.; Vladimir, K. Structure, Synthesis, and Catalytic Performance of Emerging MXene-Based Catalysts. *Molecules* **2024**, *29*, 1286. [CrossRef] [PubMed]

67. Jakubczak, M.; Bury, D.; Wojciechowska, A.; Karwowska, E.; Jastrzębska, A.M. Excellent antimicrobial and photocatalytic performance of C/GO/TiO_2/Ag and C/TiO_2/Ag hybrid nanocomposite beds against waterborne microorganisms. *Mater. Chem. Phys.* **2023**, *297*, 127333. [CrossRef]
68. Naguib, M.; Mashtalir, O.; Carle, J.; Presser, V.; Lu, J.; Hultman, L.; Gogotsi, Y.; Barsoum, M.W. Two-dimensional transition metal carbides. *ACS Nano* **2012**, *6*, 1322–1331. [CrossRef]
69. Halim, J.; Kota, S.; Lukatskaya, M.R.; Naguib, M.; Zhao, M.Q.; Moon, E.J.; Pitock, J.; Nanda, J.; May, S.J.; Gogotsi, Y.; et al. Synthesis and Characterization of 2D Molybdenum Carbide (MXene). *Adv. Funct. Mater.* **2016**, *26*, 3118–3127. [CrossRef]
70. Naguib, M.; Barsoum, M.W.; Gogotsi, Y. Ten Years of Progress in the Synthesis and Development of MXenes. *Adv. Mater.* **2021**, *33*, e2103393. [CrossRef]
71. Tariq, A.; Ali, S.I.; Akinwande, D.; Rizwan, S. Efficient Visible-Light Photocatalysis of 2D-MXene Nanohybrids with $Gd^{(3+)}$- and $Sn^{(4+)}$-Codoped Bismuth Ferrite. *ACS Omega* **2018**, *3*, 13828–13836. [CrossRef] [PubMed]
72. Jyoti, K.; Singh, A. Green synthesis of nanostructured silver particles and their catalytic application in dye degradation. *J. Genet. Eng. Biotechnol.* **2016**, *14*, 311–317. [CrossRef]
73. Zhao, Q.; Wang, J.; Li, Z.; Guo, Y.; Tang, B.; Abudula, A.; Guan, G. Two-dimensional $Ti_3C_2T_x$ -nanosheets/Cu_2O composite as a high-performance photocatalyst for decomposition of tetracycline. *Carbon Resour. Convers.* **2021**, *4*, 197–204. [CrossRef]
74. Wang, L.; Lu, F.; Liu, Y.; Wu, Y.; Wu, Z. Photocatalytic degradation of organic dyes and antimicrobial activity of silver nanoparticles fast synthesized by flavonoids fraction of *Psidium guajava* L. leaves. *J. Mol. Liq.* **2018**, *263*, 187–192. [CrossRef]
75. Naraginti, S.; Stephen, F.B.; Radhakrishnan, A.; Sivakumar, A. Zirconium and silver co-doped TiO_2 nanoparticles as visible light catalyst for reduction of 4-nitrophenol, degradation of methyl orange and methylene blue. *Spectrochim. Acta A Mol. Biomol. Spectrosc.* **2015**, *135*, 814–819. [CrossRef]
76. Kumari, R.M.; Thapa, N.; Gupta, N.; Kumar, A.; Nimesh, S. Antibacterial and photocatalytic degradation efficacy of silver nanoparticles biosynthesized using Cordia dichotomaleaf extract. *Adv. Nat. Sci. Nanosci. Nanotechnol.* **2016**, *7*, 045009. [CrossRef]
77. Chen, S.; Liu, R.; Kuai, Z.; Li, X.; Lian, S.; Jiang, D.; Tang, J.; Li, L.; Wu, R.; Peng, C. Facile synthesis of a novel $BaSnO_3$/MXene nanocomposite by electrostatic self-assembly for efficient photodegradation of 4-nitrophenol. *Environ. Res.* **2022**, *204*, 111949. [CrossRef]
78. Liu, X.; Li, W.; Chen, N.; Xing, X.; Dong, C.; Wang, Y. Ag–ZnO heterostructure nanoparticles with plasmon-enhanced catalytic degradation for Congo red under visible light. *RSC Adv.* **2015**, *5*, 34456–34465. [CrossRef]
79. Karthika, V.; Arumugam, A.; Gopinath, K.; Kaleeswarran, P.; Govindarajan, M.; Alharbi, N.S.; Kadaikunnan, S.; Khaled, J.M.; Benelli, G. Guazuma ulmifolia bark-synthesized Ag, Au and Ag/Au alloy nanoparticles: Photocatalytic potential, DNA/protein interactions, anticancer activity and toxicity against 14 species of microbial pathogens. *J. Photochem. Photobiol. B Biol.* **2017**, *167*, 189–199. [CrossRef]
80. Liu, Q.; Tan, X.; Wang, S.; Ma, F.; Znad, H.; Shen, Z.; Liu, L.; Liu, S. Correction: MXene as a non-metal charge mediator in 2D layered CdS@Ti_3C_2@TiO_2 composites with superior Z-scheme visible light-driven photocatalytic activity. *Environ. Sci. Nano* **2019**, *6*, 3170. [CrossRef]
81. Bhakya, S.; Muthukrishnan, S.; Sukumaran, M.; Muthukumar, M.; Kumar, S.T.; Rao, M.V. Catalytic Degradation of Organic Dyes using Synthesized Silver Nanoparticles: A Green Approach. *J. Bioremediation Biodegrad.* **2015**, *6*, 1. [CrossRef]
82. Rasheed, T.; Rasheed, A.; Munir, S.; Ajmal, S.; Muhammad Shahzad, Z.; Alsafari, I.A.; Ragab, S.A.; Agboola, P.O.; Shakir, I. A cost-effective approach to synthesize $NiFe_2O_4$/MXene heterostructures for enhanced photodegradation performance and anti-bacterial activity. *Adv. Powder Technol.* **2021**, *32*, 2248–2257. [CrossRef]
83. Teimouri, M.; Khosravi-Nejad, F.; Attar, F.; Saboury, A.A.; Kostova, I.; Benelli, G.; Falahati, M. Gold nanoparticles fabrication by plant extracts: Synthesis, characterization, degradation of 4-nitrophenol from industrial wastewater, and insecticidal activity–A review. *J. Clean. Prod.* **2018**, *184*, 740–753. [CrossRef]
84. Chandiran, K.; Pandian, M.S.; Balakrishnan, S.; Pitchaimuthu, S.; Chen, Y.-S.; Nagamuthu Raja, K.C. $Ti_3C_2T_x$ MXene decorated with $NiMnO_3$/$NiMn_2O_4$ nanoparticles for simultaneous photocatalytic degradation of mixed cationic and anionic dyes. *Colloids Surf. A Physicochem. Eng. Asp.* **2024**, *692*, 133888. [CrossRef]
85. Mei, J.; Zhang, L.; Niu, Y. Fabrication of the magnetic manganese dioxide/graphene nanocomposite and its application in dye removal from the aqueous solution at room temperature. *Mater. Res. Bull.* **2015**, *70*, 82–86. [CrossRef]
86. Chandra, S.; Das, P.; Bag, S.; Bhar, R.; Pramanik, P. Mn_2O_3 decorated graphene nanosheet: An advanced material for the photocatalytic degradation of organic dyes. *Mater. Sci. Eng. B* **2012**, *177*, 855–861. [CrossRef]
87. Ullah, K.; Ye, S.; Zhu, L.; Meng, Z.-D.; Sarkar, S.; Oh, W.-C. Microwave assisted synthesis of a noble metal-graphene hybrid photocatalyst for high efficient decomposition of organic dyes under visible light. *Mater. Sci. Eng. B* **2014**, *180*, 20–26. [CrossRef]
88. Faheem, M.; Riaz, A.; Alam, M.; Wahad, F.; Sohail, M.; Altaf, M.; Abbas, S.M. 2D Nanostructured MXene-Based Silver Nanoparticles for Photocatalytic Degradation of Safranin Dye. *Catalysts* **2024**, *14*, 201. [CrossRef]
89. Romman, U.E.; Shakir, I.; Shaaban, I.A.; Assiri, M.A.; Chaudhary, K.; Warsi, M.F.; Shahid, M. Silver-doped lanthanum nickel oxide decorated $Ti_3C_2T_x$ MXene nano-composite (Ag–$LaNiO_3$/MXene) for advanced photocatalytic waste-water treatment. *Opt. Mater.* **2024**, *147*, 114678. [CrossRef]
90. Othman, Z.; Sinopoli, A.; Mackey, H.R.; Mahmoud, K.A. Efficient Photocatalytic Degradation of Organic Dyes by AgNPs/$Ti_3C_2T_x$ MXene Composites under UV and Solar Light. *ACS Omega* **2021**, *6*, 33325–33338. [CrossRef] [PubMed]

91. Fu, X.; Kong, Y.; Wang, M.; Cai, T.; Zeng, Q. MXene derived $Ti_3C_2T_x$ /Ag persistent photocatalyst with enhanced electron storage capacity for round-the-clock degradation of organic pollutant. *J. Colloid Interface Sci.* **2024**, *656*, 233–240. [CrossRef] [PubMed]
92. Roy, I.; Rana, D.; Sarkar, G.; Bhattacharyya, A.; Saha, N.R.; Mondal, S.; Pattanayak, S.; Chattopadhyay, S.; Chattopadhyay, D. Physical and electrochemical characterization of reduced graphene oxide/silver nanocomposites synthesized by adopting a green approach. *RSC Adv.* **2015**, *5*, 25357–25364. [CrossRef]
93. Chand, K.; Cao, D.; Fouad, D.E.; Shah, A.H.; Lakhan, M.N.; Dayo, A.Q.; Sagar, H.J.; Zhu, K.; Mohamed, A.M.A. Photocatalytic and antimicrobial activity of biosynthesized silver and titanium dioxide nanoparticles: A comparative study. *J. Mol. Liq.* **2020**, *316*, 113821. [CrossRef]